Impact of Meteorology and Aerosol Sources on PM$_{2.5}$ and Oxidative Potential Variability and Levels in China

Jiemei Liu[1,2], Jesper H. Christensen[2], Zhuyun Ye[2], Shikui Dong[1], Camilla Geels[2], Jørgen Brandt[2], Athanasios Nenes[3,4], Yuan Yuan[1, *], and Ulas Im[2, *]

5   [1] Key Laboratory of Aerospace Thermophysics, Ministry of Industry and Information Technology, Harbin Institute of Technology, 92 West Dazhi Street, Harbin 150001, China

[2] Aarhus University, Department of Environmental Science/Interdisciplinary Centre for Climate Change, Frederiksborgvej 399, Roskilde, Denmark

[3] Laboratory of Atmospheric Processes and Their Impacts, Ecole Polytechnique Fédérale de Lausanne

10   (EPFL), Lausanne, Switzerland

[4] Center for the Study of Air Quality and Climate Change, Foundation for Research and Technology Hellas (FORTH), Thessaloniki, Greece,

Correspondence: Yuan Yuan (yuanyuan83@hit.edu.cn) and Ulas Im (ulas@envs.au.dk)

Abstract: China has long-term high PM$_{2.5}$ levels, and its Oxidative Potential (OP) is worth studying as it may unravel the impacts of aerosol pollution on public health better than PM$_{2.5}$ alone. OP and PM$_{2.5}$ are influenced by meteorological factors, anthropogenic emissions sources and atmospheric aging. Although their impact on PM$_{2.5}$ have been studied, OP measurements only recently became available and on a limited scale, as they require considerable technical expertise and resources. For this, the joint relationship between PM$_{2.5}$ and OP for a wide range of meteorological conditions and emissions profiles remain elusive. Towards this, we estimated PM$_{2.5}$ and OP over China using the Danish Eulerian Hemispheric Model (DEHM) system with meteorological input from WRF weather forecast model. It was found that higher values of PM$_{2.5}$ and OP were primarily concentrated in urban agglomerations in the central and eastern regions of China, while lower values were found in the western and northeastern regions. Furthermore, the probability density function revealed that about 40% of areas in China had an annual average PM$_{2.5}$ concentrations exceeding the Chinese concentrations limit; 36% of the regions have OP below 1 $nmol\ min^{-1}\ m^{-3}$, 41% have OP between 1 and 2 $nmol\ min^{-1}\ m^{-3}$, and 23% have OP above 2 $nmol\ min^{-1}\ m^{-3}$. Analysis of the simulations indicate that meteorological conditions and anthropogenic emission contributed 46% (65%) and 54% (35%) to the PM$_{2.5}$ concentration (OP) variability. The emission sensitivity analysis also highlighted PM$_{2.5}$ and OP levels are mostly determined by secondary aerosol formation and biomass burning.

Keywords: PM$_{2.5}$; Oxidative potential; Meteorology; Anthropogenic emission sources; Probability density function

1. Introduction

Fine particulate matter, with an aerodynamic diameter of less than 2.5 μm ($PM_{2.5}$), is the primary atmospheric pollutant in China (Chen et al., 2021; Chen et al., 2021; Liu et al., 2023) with respect to human health. $PM_{2.5}$ exposure in China for 2017 resulted in an estimated 1.8 (95% CI: 1.6, 2.0) million premature deaths (Liu et al., 2021). Many recent studies have suggested that the oxidative potential (OP) of $PM_{2.5}$ (the ability of $PM_{2.5}$ to produce reactive oxygen species (ROS) to *in-vitro* that consume intracellular antioxidants; (Campbell et al., 2021)) may better explain the negative impact of $PM_{2.5}$ exposure on human health than the well-established metric of mass concentrations (Yu et al., 2019; Gao et al., 2020). This is because exposure to high levels of OP (from compounds such as quinones and soluble transitional metals) induces an excess production of ROS in cells and lead to oxidative stress (OS) effects and ultimately trigger inflammation and disease. Therefore, reducing $PM_{2.5}$ pollution and its associated OP (the volume-normalized dithiothreitol activity) are critical to addressing China's environmental and environmental health issues.

Anthropogenic emissions, as the main source of $PM_{2.5}$ pollution and environmental health risks, have been studied extensively (Chen et al., 2019; Liu et al., 2022). Zhu et al. (2018) and Pui et al. (2014) summarized the studies on the PM sources in China and reported that secondary inorganic aerosols (SIA), industry, residential combustion, biomass burning, industry, and transportation are the main source categories in China in the historical and future business-as-usual scenarios. Due to the significant influence of various sectors on $PM_{2.5}$ emissions, and research (Liu et al., 2018; Liu et al., 2020) indicating a close association between $PM_{2.5}$ and OP, the connection between OP, serving as a toxicity indicator for $PM_{2.5}$, and its sources (Liu et al., 2020) is becoming increasingly crucial and the topic of numerous studies. For instance, Yu et al. (2019) used the dithiothreitol (DTT) assay to measure the $PM_{2.5}$ samples in Beijing throughout the year and identified vehicle emissions as the main contributing source based on the source analysis of OP. However, studies conducted in three coastal cities of the Bohai Sea region (Liu et al., 2018) and in Nanjing (Zhang et al., 2023) using the same DTT assay indicated that coal combustion was the most active source of OP. Together, these studies suggest that obtaining the spatial distribution characteristics of $PM_{2.5}$ and OP and their links to emission sources, is of paramount importance for implementing region-specific control measures.

Apart from anthropogenic emissions, meteorological conditions (i.e., temperature, humidity, wind speed, precipitation) also play a crucial role in the formation, accumulation, transformation, and dispersion of $PM_{2.5}$ (Liu et al., 2022; Liu et al., 2022). Utilizing a multiple linear regression model, Gong et al. (2022) conducted an analysis of the trends of meteorological elements and $PM_{2.5}$ levels across various regions in China from 2013 to 2020. Furthermore, they separated and quantified the impacts of meteorological factors and emissions on these trends. The findings indicate that meteorology alone can account for approximately 20~33% of the variability in $PM_{2.5}$ levels. Xing et al. (2023) conducted a study in the Shenzhen region using DTT, ascorbic acid (AA), and glutathione (GSH) OP assays. They analyzed meteorological conditions and $PM_{2.5}$ chemical composition to understand how the prevalence of monsoons in winter (northern and northeastern winds) and summer (southern and southeastern winds) affected the sources and contributed to the seasonal variation in $PM_{2.5}$ composition and OP (mass-normalized). Similarly, Molina et al. (2023) and Wang et al. (2019) revealed that meteorological conditions indirectly influence OP (volume-normalized and mass-normalized) through their impact on the chemical properties of the components. Ainur et al. (2023) employing a DTT assay, investigated outdoor health risks associated with atmospheric particulate matter in Xi'an, find a positive correlation between winter OP (volume-normalized) and relative humidity. Although several studies have identified linkages between meteorological conditions and $PM_{2.5}$/OP, quantitative assessment of meteorological conditions to both $PM_{2.5}$ and OP variability is lacking.

As of the present, research on the influence of both meteorological conditions and anthropogenic emissions on OP primarily relies on measurement methods (Yu et al., 2019; Gao et al., 2020; Campbell et al., 2021), such as DTT, AA, and GSH, which are difficult and costly to test and hard to provide the spatial distribution of OP comprehensively. Although mechanistic models of OP do exist (Shahpoury et al., 2024), their links to experimental metrics of OP are qualitative. For this, we propose a hybrid approach combing existing observations of OP with a chemistry transport model (CTM). So, using OP from assays and their observed links to sources and chemical constituents can then be parameterized and implemented in CTM for a comprehensive assessment of OP exposure over large areas and time periods.

This study quantifies the contribution of meteorological and anthropogenic emission factors (i.e., coal combustion, biomass burning, secondary aerosol formation that originate from a series of atmospheric reactions, industry, and transportation source) to OP and $PM_{2.5}$ levels throughout China with the Danish Eulerian Hemispheric Model (DEHM) model. The study hence provides a method for calculating OP

across China and using OP as an indicator to assess the impacts of anthropogenic emission sources on

95 human health in China.

2. Materials and methods

2.1 Methodological flow

The research strategy of this study consists of three main parts: model setup, spatial distribution

characteristic analysis, and quantification of meteorological conditions and anthropogenic emissions'

100 contributions (Figure 1). In the first part, DEHM was employed to obtain hourly pollutant concentrations,

followed by model evaluation, where the numerical weather prediction model WRF v4.1 (Skamarock et

al., 2008) driven by ERA5 was used as meteorological input to DEHM and with exactly same spatial

setup for China as in DEHM. Sensitivity experiments were designed for meteorological conditions,

emission inventories, and anthropogenic emission sources. From these simulations, the spatial-scale

105 estimation of OP was conducted using model outputs and the relationship between OP (this study focuses

on the volume-normalized dithiothreitol activity) and $PM_{2.5}$ concentrations from various anthropogenic

sources (Zheng et al., 2018; Tong et al., 2018; Yun et al., 2020; MEE, 2020; Wang et al., 2020; Tang

et al., 2020; Lin et al., 2021; Chen et al., 2022).
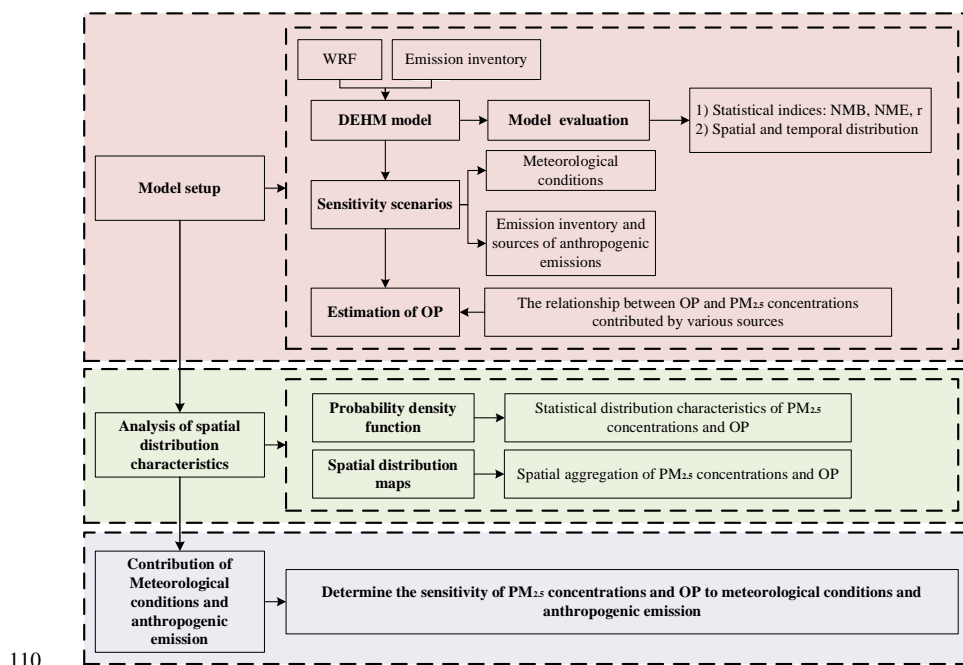
Figure 1. Schematic diagram of the study strategy; NME, NMB, r, and OP are normalized mean error, normalized mean bias, correlation coefficient, and oxidative potential, respectively.

In the second part, the spatial distribution characteristics of PM$_{2.5}$ and OP were determined using probability density functions (PDF) and spatial distribution maps. In the third part, quantitative analysis was conducted based on the simulation results from the sensitivity experiments to determine the extent of influence of meteorology and emissions on PM$_{2.5}$ and OP, as well as the primary sources of PM$_{2.5}$ and OP.

2.2 Model setup

The DEHM can well capture many features of PM and its precursors' changes in large-scale space (Christensen, 1997; Brandt et al., 2012; Im et al., 2019). To date, the DEHM model has been widely used in air pollution and health risk assessment research in Europe and Asia (Brandt et al., 2013a; b; Zare et al., 2014; Geels et al., 2015; Im et al., 2018; Im et al., 2019; Lehtomäki et al., 2020; Cramer et al., 2020; Liu et al., 2021; Geels et al., 2021; Thomas et al., 2022; Im et al., 2023), but this will be the first time that DEHM is applied to estimate OP. Thus, The DEHM model system was used to simulate the pollutant concentrations in 2014 by using a two-way nested domain in this study (Kumar et al., 2016). A mother domain with a resolution of 150 km ×150 km was employed on a polar stereographic projection,

true at 60 ̊N to cover the entire Northern Hemisphere. The nested domain covered the whole of China

consisting of 150×150 grid cells with a resolution of 50 km $\times$ 50 km. Vertically, there were 29 unevenly

distributed layers, with the highest level reaching 100 hPa, and the lowest layer was approximately 20 m

130   in height. The meteorological fields were simulated using the WRF model (Skamarock et al., 2008)

with the same domain and resolution driven by global reanalysis as ERA5 or global climate data from

CESM. The time resolution of the DEHM model output is one hour. The gas-phase chemistry module

included 66 species, 9 primary particles (including natural particles such as sea salt), and 138 chemical

reactions (Brandt et al., 2012). The secondary organic aerosols (SOA) were calculated using the

135   volatility basis set (see details in Im et al. (2019)). In addition to the anthropogenic emissions, DEHM

also includes emissions from biogenic emissions, such as vegetation, sea salt, lightning, soil, etc. The

current version of the DEHM model does not include wind-blown, resuspended dust emissions or road

dust.

In the current study, the DEHM model used anthropogenic emissions from the Emissions Database for

140   Global Atmospheric Research – Hemispheric Transport of Air Pollution (EDGAR-HTAP) database and

biogenic emissions are calculated online based on the Model of Emissions of Gases and Aerosols from

Nature (MEGAN) (see details in Im et al. (2019)).

2.3 Estimation of OP

Most of current data on OP of PM$_{2.5}$ in China are obtained by means of measurement, and the research

145   objects are basically limited to specific cities, which to some extent hinders the conduct of research on

OP in a large-scale region. Considering that Liu et al. (2018) collected samples across four seasons from

multiple representative locations in China, their developed OP prediction model (Equation (1)) can

support us in estimating OP in China, thereby exploring the spatial distribution characteristics of OP and

the contributions of different anthropogenic sources to OP. In the present study, we have used this

150   relationship, in combination with the sensitivity simulations (section 2.4), to calculate the OP.

$$OP = 0.088 \times re + 0.076 \times bi + 0.041 \times se + 0.034 \times in + 0.017 \times tr \qquad (1)$$

where, re, bi, in, and tr represent the primary PM$_{2.5}$ concentrations for coal combustion, biomass

burning, industry source, and transportation source, respectively. In this study, the coal combustion is

primarily from heating during the local cold season. Biomass burning includes open burning of

agricultural biomass, domestic biomass burning for cooking and heating, and biomass burning from

155   power plants. Industry source is primarily from specific industry processes. Transportation source

primarily comes from pipe emissions. *se* (secondary aerosol formation) refers to the concentrations of

secondary organic and inorganic (SOA and SIA, respectively) components. It's worth mentioning that

secondary aerosol formation originates from a series of atmospheric reactions. Some identified sources

(i.e., coal combustion, biomass burning, industrial processes, and transportation) may generate secondary

160   inorganic and organic aerosols through the emission of their precursor components. Therefore,

coefficient reflect the intrinsic OP of each source.

2.4 Sensitivity scenarios

2.4.1 Relative contributions from meteorological conditions and emissions

165   Table 1 summarizes the scenarios for assessing the relative contributions of meteorological conditions

and emissions to PM$_{2.5}$ and OP variability in 2014. Scenarios C$_1$ and C$_2$ used the same meteorological

reanalyse dataset (ERA5) as input to WRF, while Scenario C$_3$ utilized CESM climate model based

meteorological data as input. ERA5 (Hersbach et al., 2020; ERA, 2023) is a global reanalysis dataset

that is based on the assimilation of historical observations and model data. CESM (2023), on the other

170   hand, is a global climate and Earth system model supported by the US National Science Foundation, and

its meteorological outputs serve as inputs for the WRF model as well. CESM version 2.1.1 (Danabasoglu

et al., 2020) was first ran from 1850-2015 with the standard input component set BHISTcmip6 on

f09_g17 resolution (i.e., 0.9°x1.25° resolution). Scenarios C$_2$ and C$_3$ employed the Eclipse V6 emissions

inventory, while Scenario C$_1$ used the EDGAR-HTAP inventory.

175   The ECLIPSE project by the International Institute for Applied Systems Analysis (IIASA) aims to

generate a global gridded anthropogenic emission inventory for various emission scenarios. The

Greenhouse Gas - Air Pollution Interactions and Synergies (GAINS) model has been employed to

estimate emissions using source characteristics and emission factors at a resolution of 0.5 °x 0.5 °latitude-

longitude (Upadhyay et al., 2020; Eclipse, 2020). The following sector-layers are available: energy,

180   industry, solvent use, transport, domestic combustion, agriculture, open burning of agricultural waste,

waste treatment. a number of scenarios are provided for which the key economic assumptions and energy

use originate from IEA World Energy Outlook (IEA, 2011), the POLES model, or Energy Technology

Perspectives (IEA, 2012) for the period 2010-2050, while statistical data for the period 1990-2010 came

from IEA. For agriculture the FAO databases and long-term global projections were used (Alexandratos

et al., 2012). It is noteworthy that this inventory takes into account China 13th 5-year plan. The

EDGAR-HTAP (Joint et al., 2011; Crippa et al., 2023) emission inventory endeavors to employ official

or scientific inventories within a national or regional scale, with a spatial resolution of $0.1° \times 0.1°$. The

temporal coverage spans from the year 2000 to 2018. EDGAR-HTAP comprehensively accounts for all

major emission sectors, including residential, transportation, industrial, energy, and agricultural sectors.

Equations (2~5) were used to quantitatively evaluate the contributions of meteorological conditions and

emission inventories.

$$\text{Con(Met)} = \frac{C_2 - C_3}{C_3} \tag{2}$$

$$\text{Con(Emi)} = \frac{C_1 - C_2}{C_2} \tag{3}$$

$$\text{NCon(Met)} = \frac{\text{abs(Con(Met))}}{\text{abs(Con(Met))} + \text{abs(Con(Emi))}} \tag{4}$$

$$\text{NCon(Emi)} = \frac{\text{abs(Con(Emi))}}{\text{abs(Con(Met))} + \text{abs(Con(Emi))}} \tag{5}$$

where, C_1, C_2 and C_3 represent the PM$_{2.5}$ concentrations and OP from scenarios C_1, C_2 and C_3,

respectively. Con(Met) represents the impact of changing meteorological datasets on changes in PM$_{2.5}$

and OP. Con(Emi) represents the impact of changing emission inventory on changes in PM$_{2.5}$ and OP.

abs represents the absolute value. NCon(Met) and NCon(Emi) represent the normalized contributions of

meteorology and emission.

Table 1. Emission inventory and meteorological datasets in three simulation scenarios.

Scenarios	Emission inventory	Meteorological datasets
C_1	EDGAR-HTAP	ERA5
C_2	Eclipse V6	ERA5
C_3	Eclipse V6	CESM

2.4.2 Relative contributions from individual emissions

As mentioned above, OP's main source contributions include five parts, i.e., coal combustion, biomass

burning, secondary aerosol formation, industrial sources, and transportation sources (Equation (1)), we

conducted perturbation experiments targeting these five sources to quantitatively assess their

contributions to PM$_{2.5}$ concentration and OP(Figure 2). These experiments were carried out within the

three scenarios proposed in Section 2.4.1, and we performed a total of 15 runs. Under the non-

perturbation condition (referred to as the NPC case), all aforementioned emission sources were

205 considered. Under the perturbation condition (referred to as the PC case), reduction designs were

implemented for emissions from coal combustion, biomass burning, industrial sources, and

transportation sources. The emission from each individual source is reduced by 30%. Notably, to estimate

the PM$_{2.5}$ concentrations and OP from coal and biomass burning, it is necessary to obtain the percentage

contributions of PM$_{2.5}$ emissions from coal combustion for residential heating, domestic biomass burning

210 for cooking and heating to PM$_{2.5}$ emissions of the residential sector, respectively, as well as the

percentage contributions of PM$_{2.5}$ emissions from biomass combustion in power plants to the total PM$_{2.5}$

emissions from the power sector. The percentage contributions of each anthropogenic source can be

estimated using Equations (6~8).

$$PC_{re_{-j}} = \frac{E_{re\_j}}{E_{re}} \tag{6}$$

$$E_{pp_{-bi}} = EF \times FQ \tag{7}$$

$$PC_{pp\_bi\_cf} = \frac{E_{pp_{-bi}} + E_{pp\_cf}}{E_{pp}} \tag{8}$$

where, $PC_{re_{-j}}$ denotes the percentage contribution of PM$_{2.5}$ emissions from the residential subsector j

215 (including coal cooking, coal heating, biomass cooking, biomass heating, clean energy, and

nonresidential) to the total PM$_{2.5}$ emissions from the residential sector. E_{re_j} represents the PM$_{2.5}$

emissions from the residential subsector j, while E_{re} represents the total PM$_{2.5}$ emissions from the

residential sector. The values of E_{re_j} and E_{re} are obtained from the literature (Yun et al., 2020). $E_{pp_{-bi}}$

refers to the PM$_{2.5}$ emissions from biomass power plants, EF refers to the PM$_{2.5}$ emission factor of

220 biomass power plants, and FQ refers to the fuel quantity. $PC_{pp\_bi\_cf}$ refers to the percentage contribution

of PM$_{2.5}$ emissions from biomass power plants and coal-fired power plants to the PM$_{2.5}$ emissions of the

power plants. E_{pp_cf} refers to the PM$_{2.5}$ emissions from coal-fired power plants, and E_{pp} refers to the

PM$_{2.5}$ emissions from power plants. EF, FQ, E_{pp_cf}, and E_{pp} are obtained from the literature (Zheng et

al., 2018; Tong et al., 2018; Yun et al., 2020; MEE, 2020; Wang et al., 2020; Tang et al., 2020; Lin

225 et al., 2021; Chen et al., 2022). More and more studies (Hodan et al., 2004; Chen et al., 2018; Zhang

et al., 2022) showed that in China, the proportion of secondary and primary PM$_{2.5}$ mass to the total PM$_{2.5}$

mass is close, so we assume that they account for 50% respectively. Figure 2 showed the emission

reduction design for perturbed emissions.
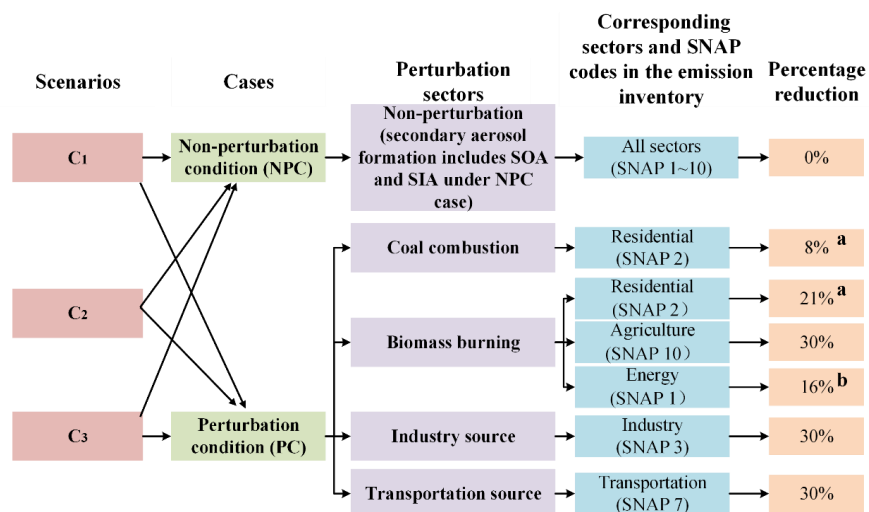
Figure 2. Emission reduction design for perturbed emissions; [a] was obtained from the literature (Yun et al., 2020), [b] were obtained from the literature (Zheng et al., 2018; Tong et al., 2018; Yun et al., 2020; MEE, 2020; Wang et al., 2020; Tang et al., 2020; Lin et al., 2021; Chen et al., 2022).

Furthermore, the PM$_{2.5}$ concentration for each sector is calculated using Equations (9~11).

$$C_{P,i} = \frac{C_{NPC,i} - C_{PC,i}}{30\%} \tag{9}$$

$$C_{P,primary\ PM2.5} = C_{P,total\ PM2.5} - C_{P,SIA} - C_{P,SOA} \tag{10}$$

$$C_{secondary} = C_{NPC,SOA} + C_{NPC,SIA} \tag{11}$$

where, *i* refers to the type of pollutants, i.e., total PM$_{2.5}$, SOA, SIA, and primary PM$_{2.5}$. $C_{NPC,i}$ represents concentrations of the pollutant *i* in the NPC case. $C_{PC,i}$ represents concentrations of the pollutant *i* in the PC case. $C_{P,i}$ represents concentrations of the pollutant *i* by the specific emission sector P which is perturbed (perturbation sectors P include coal combustion, biomass burning, industry, traffic source). $C_{P,primary\ PM2.5}$ represents concentrations of primary PM$_{2.5}$ by the perturbation sectors P. $C_{secondary}$ represents PM$_{2.5}$ concentrations by the secondary aerosol formation.

2.5 Probability density function

Taking into account the substantial spatial heterogeneity of PM$_{2.5}$ concentration and OP, we employ probability distribution functions (PDF) to characterize the statistical distribution characteristics of PM$_{2.5}$

concentration and OP across China. This offers a more generalized and robust probability for criteria

limits. In this study, all three functional types (Lognormal, exponential, and Gamma) were tested for

245   annual average of $PM_{2.5}$ concentrations and OP at the monitoring stations. To determine the

representative distributions for the datasets, we further performed goodness-of-fit tests such as the Sum

of Squared Error (SSE) and the Kolmogorov-Smirnov (K-S) test (de Melo et al., 2000), using the fitter

package in Python.

3. Results and discussion

250   **3.1 Model evaluation**

The hourly observation data was obtained from the Ministry of Ecology and Environment of China (MEE,

2014). The MEE website first released $PM_{2.5}$ measurement data in January 2013. In accordance with the

Chinese environmental protection standards, the hourly $PM_{2.5}$ concentrations are measured using the

micro-oscillation balance method and beta absorption method, with an uncertainty of less than

255    $5 \ \mu g \ m^{-3}$ (Zeng et al., 2021). The $PM_{2.5}$ monitoring stations are primarily distributed in urban areas,

particularly in major metropolitan areas of China (Zeng et al., 2021). In 2014, the observation stations

were mainly concentrated in eastern China, while stations in western China are limited. Therefore, in the

present study, we also evaluated with the gridded annual-mean global reanalysis Dalhousie surface $PM_{2.5}$

dataset (van Donkelaar et al., 2021), which combines satellite retrievals of aerosol optical depth,

260   chemical transport modeling, and ground-based measurements for the period 1998-2019. The Dalhousie

dataset compensated for the non-uniform distribution spatially of observation stations to

comprehensively evaluate the performance of the DEHM model. The density scatter plot of model

performance and evaluation based on annual mean MEE observations and the Dalhousie dataset were

shown in Figure 3. Overall, the model performance in terms of correlation coefficient (R) and normalized

265   mean error (NME) calculated based on annual mean observations met the performance criteria suggested

by Emery et al. (2017) (NME<0.5, R>0.4), and the normalized mean bias (NMB) was also close to the

performance criteria suggested by Emery et al. (2017) (NMB< ±0.3). Compared to the observations, the

model performance in terms of R, NME, and NMB calculated based on the Dalhousie dataset was slightly

poorer but still close to the performance criteria suggested by Emery et al. (2017). Therefore, the

270   simulated annual mean $PM_{2.5}$ concentrations is considered reliable.
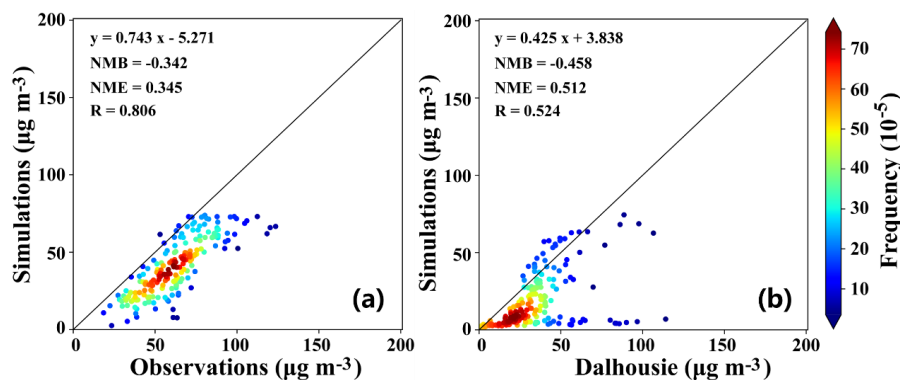
Figure 3. Density scatterplots of model performance and validation for China based on (a) MEE observations and (b) the Dalhousie dataset.

To verify the spatial accuracy, a comparison of the spatial distribution of simulated and observed PM$_{2.5}$,

275 both from MME and Dalhousie, was conducted. Figure 4 showed the spatial distribution of the difference

between simulated and MME observed values (denoted as $diff_{si-ob}$) (Figure 4a) and same for Dalhousie

dataset (denoted as $diff_{si-DH}$) (Figure 4b). Both Figure 4a and Figure 4b indicated that the majority of

regions (northeastern, central, and eastern China) exhibited differences ranging from -18 $\mu g\ m^{-3}$ to 0

$\mu g\ m^{-3}$. However, the PM$_{2.5}$ concentrations in western China are largely underestimated, and the region

280 with the worst performance has a difference reaching up to -54 $\mu g\ m^{-3}$. This is mainly due to the lack

of mineral dust emissions in the DEHM model, which is one of the main sources of pollutants in western

China. This also explains the poorer performance shown in Figure 3b. Considering that we focus on the

impact of anthropogenic emission sources on PM$_{2.5}$ concentrations and OP due to their health effects,

and that the vast majority of anthropogenic emission sources and populations are concentrated in central,

285 eastern, and northeastern China, the well performance of DEHM model in these areas demonstrate its

ability to support us exploring the role of different anthropogenic emission sources on PM$_{2.5}$

concentrations and OP in various regions, thereby identifying the main anthropogenic emission sources.
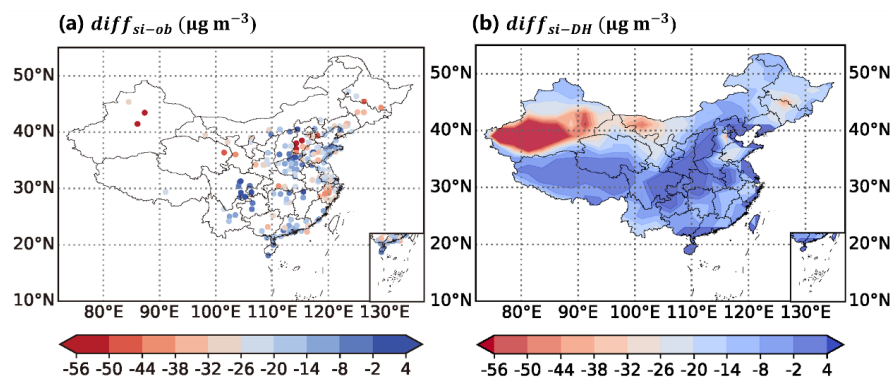
Figure 4. Spatial distribution of differences between (a) observations and (b) the Dalhousie dataset, and simulations.

Similarly, the model performance over time scales was also investigated. Scatter density plots and distribution characteristics of monthly average observations and simulations for all monitoring sites in 2014 were depicted in Figure S1 and Figure 5, respectively, with Figure S1a~ Figure S1l representing January to December. The results indicated that the simulated values were in good agreement with the observations from June to September. Although the model underestimated $PM_{2.5}$ concentrations in other months, its performance in terms of R and NME met the performance standards recommended by Emery et al. (2017) in all months except for December. We conclude that the model performs well in simulating the seasonal variation of $PM_{2.5}$ concentrations.
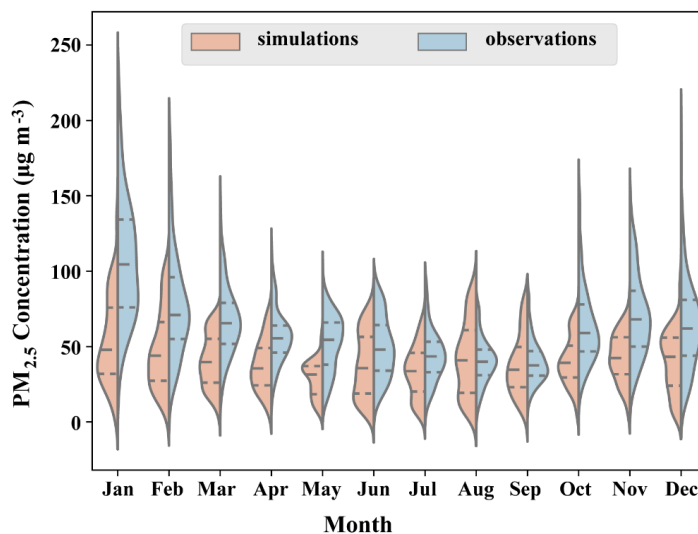
300 **Figure 5. Violin plots of monthly average observations and simulations averaged over various observation stations; The red and blue colors represent the statistical distribution of simulated and observations, respectively; The width of the violin represents the sample size; The solid black line inside the violin indicates the median. The upper and lower dashed black lines within the violin indicate the upper quartile (the 75th percentile) and lower quartile (the 25th percentile), respectively.**

305 **3.2 Spatial distribution characteristics of $PM_{2.5}$ and OP**

In order to determine the spatial distribution characteristics of $PM_{2.5}$ concentrations and OP, we explored the spatial distribution of both in scenario C_1, as shown in Figure 6a and 6b respectively. The findings demonstrated spatial clustering characteristics in $PM_{2.5}$ concentrations and OP. High $PM_{2.5}$ concentrations and High OP are mainly located in central and eastern urban clusters such as the Beijing-
310 Tianjin-Hebei region, the Shandong Peninsula, the middle reaches of the Yangtze River, the Yangtze River Delta, and the Central Plains, which have experienced rapid urbanization, industrialization, and coal burning in winter, which lead to a large amount of pollutant emissions. Low $PM_{2.5}$ concentrations and Low OP are mainly distributed in most urban areas of Xinjiang, Tibet, Qinghai, Gansu, Yunnan, Inner Mongolia, Northeast China, Pearl River Delta, Beibu Gulf, etc.

315 Due to differences in city types, pollutant emission intensities, and pollutant chemical components in different regions, there are significant spatial heterogeneity in $PM_{2.5}$ concentrations and therefore in OP. Due to high population density, socio-economic activities and winter heating needs of northern residents in China's right region, large amounts of anthropogenic emissions, especially from industry, transportation, coal burning and biomass burning, exacerbate $PM_{2.5}$ and redox active component
320 pollution.
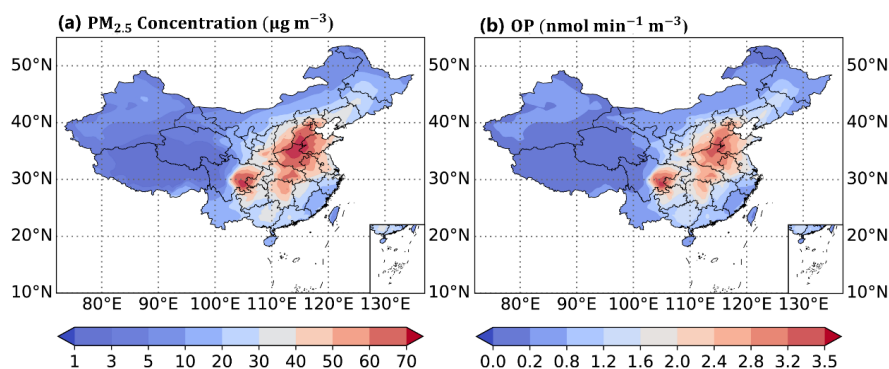
Figure 6. Spatial clustering of $PM_{2.5}$ concentrations (a) and OP (b) in China.

To quantitatively analyze the regional distribution characteristics of $PM_{2.5}$ concentrations and OP in China, we determined the distribution function that is suitable for a specific dataset (Table 3),

325 investigated the frequency histogram (FH) of $PM_{2.5}$ concentrations and OP, fitted the PDF, and then obtained the cumulative distribution function (CDF) by integrating PDF, as shown in Figure 7. It was found that the gamma distribution performed the best in fitting $PM_{2.5}$ concentrations and OP from Table 2. Considering the test results, the gamma distribution was used to explore the spatial distribution characteristics of $PM_{2.5}$ concentrations and OP. Figure 7a depicted the probability distribution of $PM_{2.5}$

330 concentrations, while Figure 7b depicted the probability distribution of OP. The wide distribution interval indicated that both $PM_{2.5}$ concentrations and OP have a similar and large spatial heterogeneity. According to the FH, the highest frequency density of $PM_{2.5}$ concentrations ranges from 10.5 to 12.9 $\mu g\ m^{-3}$; The maximum frequency density of OP ranges from 0.26 to 0.34 $nmol\ min^{-1}\ m^{-3}$. This reflects the overall pollution levels of $PM_{2.5}$ and OP in the Chinese region. Taking into account the annual average $PM_{2.5}$

335 concentrations limits set out in China's ambient air quality standard (AAQS, 2012), we focused on primary (15 $\mu g\ m^{-3}$) and secondary concentrations (35 $\mu g\ m^{-3}$) limits. The PDF and CDF results showed that 84.8% of the total area was above the primary concentrations limit and 39.7% was above the secondary concentrations limit. In addition, 35.7% of regions in China have an OP below 1.00 $nmol\ min^{-1}\ m^{-3}$, 41.3% have an OP between 1.00 and 2.00 $nmol\ min^{-1}\ m^{-3}$, and 23.0% have an OP

340 above 2.00 $nmol\ min^{-1}\ m^{-3}$.

Table 2. Goodness-of-fit test results

Item	goodness-of-fit test	Gamma	Lognormal	Exponential
$PM_{2.5}$	SSE	0.002	0.023	0.003
concentrations	KS_pvalue	0.329	0.000	0.000
OP	Sumsquare_error	0.654	0.746	1.209
	KS_pvalue	0.231	0.271	0.000

Bold values indicate the best results.

*Note:

SSE is Sum of Squared Error

KS_pvalue is the P-value of the Kolmogorov-Smirnov test
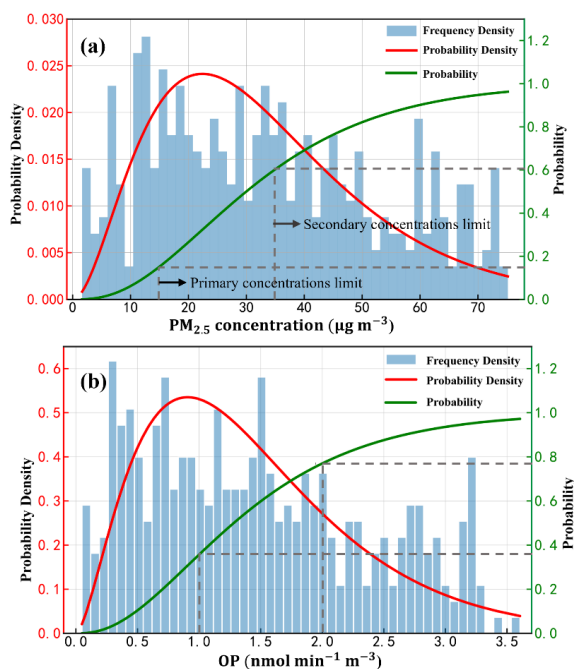
Figure 7. Probability distribution of (a) PM$_{2.5}$ concentrations and (b) OP in China

3.3 Contributions of meteorological conditions and emission inventories to the variations in PM$_{2.5}$ and OP

To determine the sensitivity of PM$_{2.5}$ pollution and oxidation potential (OP) to meteorological conditions (emission inventories), this study compared scenarios C$_2$ and C$_3$ (C$_1$) and investigated the impacts and contributions due to ERA5 and CESM (HTAP and Eclipse V6 emission inventories) on PM$_{2.5}$ and OP. Figure 8 illustrated the spatial distribution maps of PM$_{2.5}$ concentrations and OP under scenarios C$_1$, C$_2$, and C$_3$. Figure 8a~8c represented PM$_{2.5}$ concentrations under scenarios C$_1$, C$_2$, and C$_3$, respectively, while figure 8 d~8f represented OP under the same scenarios. Figure 9a presented the annual average PM$_{2.5}$ concentrations and OP under different scenarios, and Figure 9b showed the relative contributions of meteorological conditions and emission inventories. From Figures 8 and 9, it can be observed that, compared to scenario C$_2$, PM$_{2.5}$ concentrations and OP are lower in the western region and slightly higher in some eastern areas under scenario C$_1$, primarily due to changes in emission inventories attributed to the inclusion or exclusion of specific local sources during the compilation process. Compared to scenario C$_3$, PM$_{2.5}$ concentrations and OP are lower in the western region and higher in some eastern areas under

scenario C_2, primarily attributed to meteorological contributions. For the entire China region, the

transition in emission inventories from Eclipse V6 to HTAP resulted in an overall decrease in $PM_{2.5}$

360   concentrations of 1.55 $\mu g\ m^{-3}$, approximately 7.61%, and a decrease in OP of 0.0339 $nmol\ min^{-1}\ m^{-3}$,

approximately 4.05%. The shift in meteorological data from CESM to ERA5 led to an increase in $PM_{2.5}$

concentrations of 1.22 $\mu g\ m^{-3}$, approximately 6.4%, and an increase in OP of 0.0585 $nmol\ min^{-1}\ m^{-3}$,

approximately 7.5%. According to the normalization process using equations (4)~(5), meteorological

conditions contributed approximately 45.6% to the variations in $PM_{2.5}$ and approximately 65.0% to the

365   variations in OP. Meanwhile, emission inventories contributed approximately 54.4% to the variations in

$PM_{2.5}$ and approximately 35.0% to the variations in OP. Our findings highlight the significance of the

quality of model input data, including emission inventories and meteorological data, for model

performance.
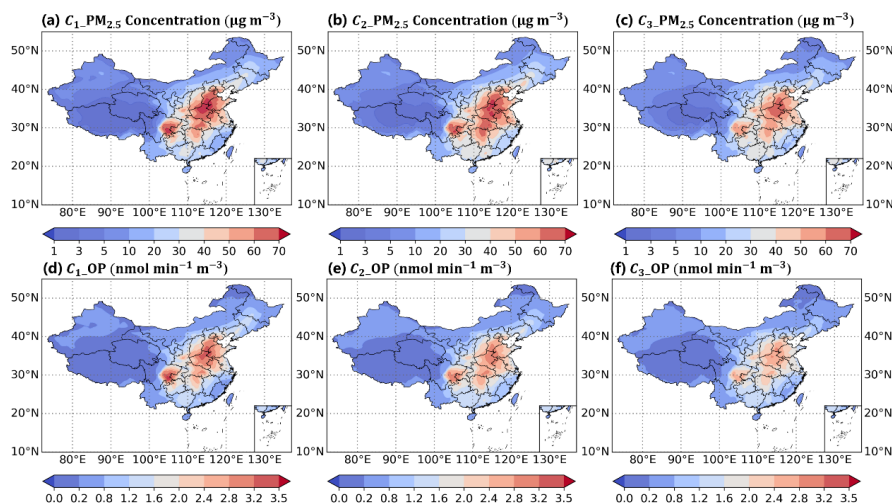
370   **Figure 8. Spatial distribution of PM$_{2.5}$ concentrations and OP in different scenarios; (a)~(c) are PM$_{2.5}$ concentrations in scenarios C$_1$, C$_2$ and C$_3$, respectively; (d)~(f) is the OP in scenarios C$_1$, C$_2$, and C$_3$, respectively; The meteorological datasets (emission inventories) employed for scenarios C$_1$, C$_2$, and C$_3$ are ERA5 (EDGAR-HTAP), ERA5 (Eclipse V6), and CESM (Eclipse V6), respectively**
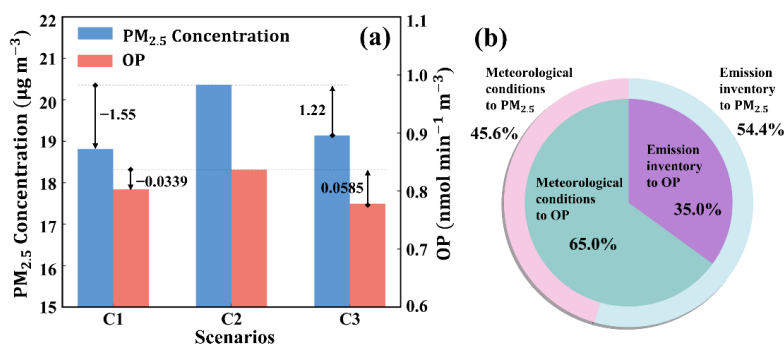
Figure 9. (a) Average annual PM₂.₅ concentrations and OP under different scenarios; (b) The relative contribution of meteorological conditions and emission inventories to PM₂.₅ and OP, with the outer circle representing PM₂.₅ and the inner circle representing OP; The meteorological datasets (emission inventories) employed for scenarios C₁, C₂, and C₃ are ERA5 (EDGAR-HTAP), ERA5 (Eclipse V6), and CESM (Eclipse V6), respectively

3.4 Contribution of anthropogenic emission sources to PM₂.₅ and OP

Considering that anthropogenic emission sources play an important role in PM$_{2.5}$ concentrations and OP, we explored the spatial distribution characteristics of PM$_{2.5}$ and OP from different anthropogenic sources to reveal the reasons behind the spatial heterogeneity in PM$_{2.5}$ concentrations and OP, as shown in Figure 10. The spatial distribution of PM$_{2.5}$ concentrations from coal combustion for residential heating, biomass combustion, secondary aerosol formation, industry, and transportation are shown in Figures 10a~10e, respectively, and same for OP are shown in Figures 10f~10j, respectively. It was evident that the spatial distribution features of PM$_{2.5}$ concentrations and OP from each emission source closely resemble those in Figure 6, and they all adhere to the principle that the eastern region is higher than the western. Nonetheless, the PM$_{2.5}$ and OP concentrations from various anthropogenic sources varied significantly across the two regions.

As seen in Figure 10, secondary aerosol formation are the primary contributors to PM$_{2.5}$ concentrations and OP. The main components of the secondary aerosol formation, such as sulfate, nitrate, ammonium salt, and water-soluble organic carbon (WSOC), are formed primarily from their precursor components, such as SO_2, NO_x, and volatile organic compounds (VOC), through a sequence of atmospheric reactions. This revealed that the role of secondary aerosol formation in OP is significant from their high contribution to mass and intrinsic OP.

Biomass combustion is mainly derived from open-air agricultural waste burning, residential biomass fuels used for heating and cooking, coal- and biomass-power plants burning (Zhang et al., 2017). It is worth noting that Chinese crops, especially corn straw, and power plants are mainly concentrated in central and eastern regions, northeast and part of the western region, which provides greater potential for biomass combustion in the eastern part of China. In addition, (Chen et al., 2023) demonstrated that aerosols emitted from biomass combustion significantly influenced the development of PBL by changing meteorological conditions, and subsequently led to the accumulation of $PM_{2.5}$ concentrations. The increase of OP is also associated with carbonaceous aerosols (Liu et al., 2020). This means that biomass burning plays a significant role in regional pollution and environmental health risks.

Coal burning increases secondary inorganic and organic aerosols in the air (Liu et al., 2018), which leads to stronger oxidative toxicity. Particularly, due to greater heating demand in locations with high population density and chilly winters, $PM_{2.5}$ concentrations and OP linked to coal burning are higher.

Industrial emissions mainly include glass manufacturing, fertilizer production, organometallic metallurgy plants and iron and steel industrial bases. This is one main source for metals. Considering the correlation between these transition metals and OP (Fang et al., 2017; Liu et al., 2018), China's four industrial zones (Liaozhong-South Heavy Industry Base, Beijing-Tianjin-Tangshan Industrial Base, Shanghai-Nanjing-Hangzhou Industrial Base, and Pearl River Delta Light Industry Base) are undoubtedly important contributors to $PM_{2.5}$ and OP emissions from industrial sources.

Transportation-related emissions encourage the accumulation of Fe, Cu, Mn, Zn, and other elements (Fang et al., 2017). Compared with other anthropogenic sources, Figure 10 demonstrated that the contribution of traffic sources to $PM_{2.5}$ and OP is the lowest, mainly concentrated in Henan, Hebei, and Shandong. This is valid for the top three provinces in terms of vehicle particulate matter and nitrogen oxide emissions in 2014 according to China Annual Vehicle Pollution Prevention and Control Report (MEE, 2015).
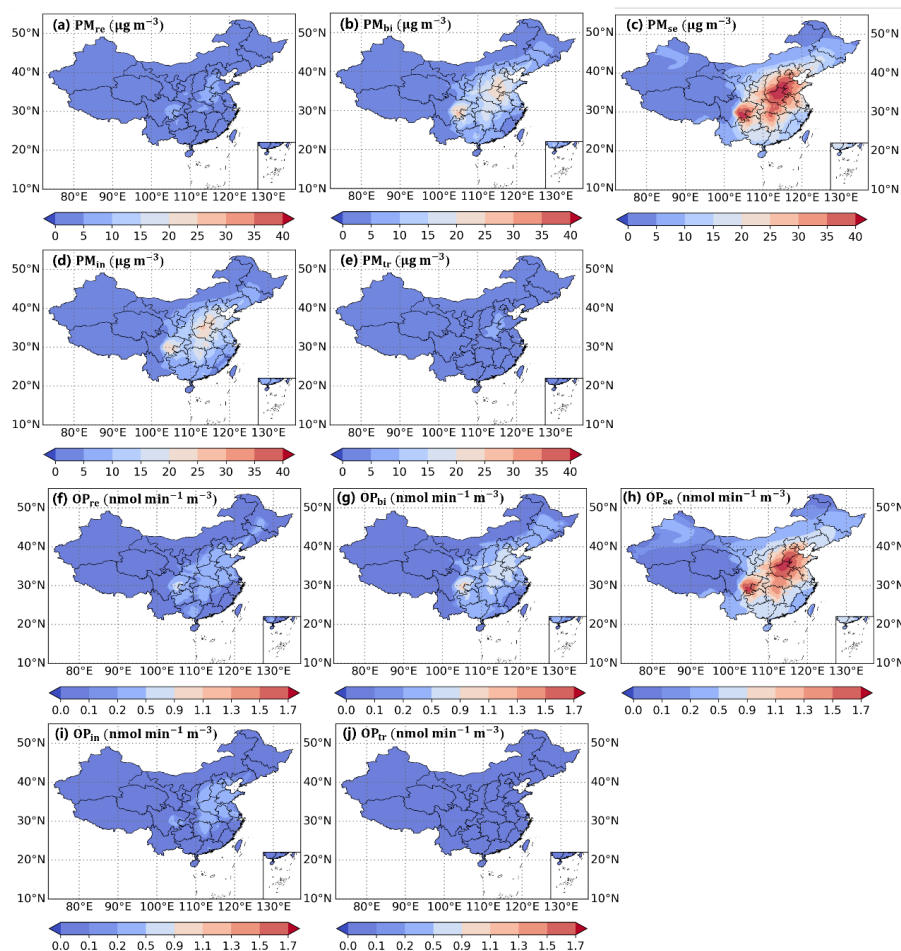
Figure 10. Spatial distribution of PM$_{2.5}$ concentrations and OP from different anthropogenic sources; (a)~(e) are PM$_{2.5}$ concentrations derived from coal combustion for residential heating (PM$_{re}$), biomass burning (PM$_{bi}$), secondary aerosol formation (PM$_{se}$), industry (PM$_{in}$), and traffic (PM$_{tr}$) respectively; (f)~(j) are the OP derived from coal combustion for residential heating (OP$_{re}$), biomass burning (OP$_{bi}$), secondary aerosol formation (OP$_{se}$), industry (OP$_{in}$), and traffic (OP$_{tr}$) respectively.

To determine the impact of anthropogenic emissions on PM$_{2.5}$ and OP, we quantified their percent contribution (Figure 11). Secondary aerosol formation, biomass combustion, industrial, coal combustion for residential heating, and transportation sources contributed 47.6%, 21.3%, 21.3%, 5.7% and 4.2% to PM$_{2.5}$, respectively. Secondary aerosol formation, biomass combustion, coal combustion for residential heating, industrial sources, and transportation sources contributed 58.0%, 21.0%, 11.1%, 8.6% and 1.2%

to OP, respectively. This means that secondary aerosol formation and biomass burning are the main sources of PM$_{2.5}$ and OP.
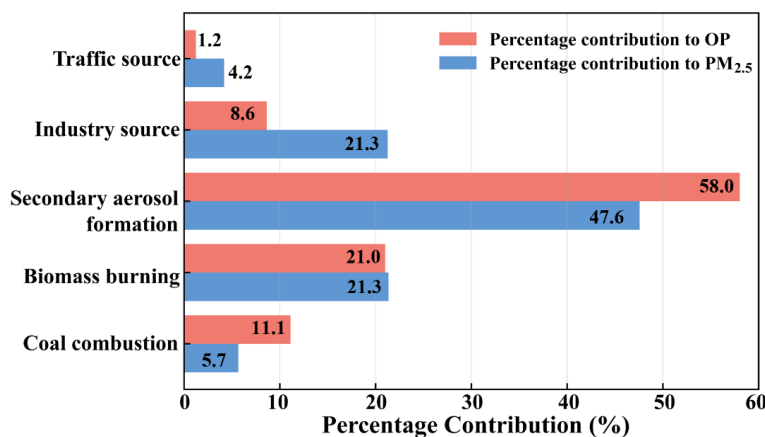
Figure 11. Percentage contribution of different anthropogenic sources.

4. Conclusions

This study established a spatial modelling for PM$_{2.5}$ concentrations and OP, provided a method for calculating OP across China, and quantitatively assessed the impacts of meteorological conditions and anthropogenic emissions on PM$_{2.5}$ and OP variability and levels in China. The following conclusions can be obtained:

- PM$_{2.5}$ and OP exhibited spatial clustering characteristics, with higher values mainly located in the central and eastern urban areas. About 85% and 40% of the areas had PM$_{2.5}$ annual average concentrations exceeding the first-grade concentrations limit (15 $\mu g\ m^{-3}$) and second-grade concentrations limit (35 $\mu g\ m^{-3}$), respectively. Additionally, about 36% of the areas had OP concentrations lower than 1 $nmol\ min^{-1}\ m^{-3}$, while 23% of the areas had OP concentrations higher than 2 $nmol\ min^{-1}\ m^{-3}$.

- Variability in both PM$_{2.5}$ and OP are influenced by a combination of meteorological conditions and emission inventories. Meteorological conditions contributed about 46% of PM$_{2.5}$ variation and 65% of OP variation. The emission inventory contributed about 54% of the change in PM$_{2.5}$ and about 35% of the change in OP.

- The percentage contributions of secondary aerosol formation, biomass burning, industry, coal combustion for residential heating, and traffic to PM$_{2.5}$ were about 48%, 21%, 21%, 6%, and 4%,

respectively. The percentage contributions of secondary aerosol formation, biomass burning, coal

455   combustion for residential heating, industry, and traffic to OP were approximately 58%, 21%, 11%,

8%, and 1%, respectively.

A main finding of this study is that meteorological variability is the prime driver of OP variability, and

not emissions. Furthermore, secondary aerosol formation and biomass burning are the main sources of

OP. Thus, air pollution strategies should focus more on biomass combustion and the emissions of the

460   precursors taking part in the secondary aerosol formation, and it would be efficient to introduce special

emissions controls during stagnation or other periods where OP accumulates.

Author contributions

465 Jiemei Liu performed the simulation and its validation, data analysis, investigation, and writing – original

draft. Jesper H. Christensen conducted investigation, worked on methodology, and performed validation.

Zhuyun Ye conducted investigation, data analysis, worked on methodology. Shikui Dong provided the

suggestion of data analysis, and manuscript feedback. Camilla Geels conducted investigation and

provided the suggestion of simulation. Jørgen Brandt conducted investigation. Athanasios Nenes

470 conducted investigation and provided manuscript feedback. Yuan Yuan provided manuscript feedback,

supervision, provided acquired funding. Ulas Im provided the resources, supervised this work, provided

manuscript feedback, and managed the project administration. All authors discussed the results and

commented on the manuscript.

Competing interests

475 The contact author has declared that none of the authors has any competing interests.

Acknowledgements:

This study was supported by the National Natural Science Foundation of China (Grant No. 52041601).

The work of Liu Jiemei was also supported by China Scholarship Council (CSC) under the State

Scholarship Fund. AN acknowledges support from the project PyroTRACH (ERC-2016-COG) funded

480 from H2020-EU.1.1. - Excellent Science - European Research Council (ERC), project ID 726165 and

from the European Union project EASVOLEE funded from HORIZON-CL5-2022-D5-01 (project ID

101095457).

Declaration of conflicting interests:

The authors declare no conflicts of interests.

485 **Supplement:**

Density scatterplots of model performance and validation based on monthly mean observations (Figure

S1) is provided in the Supplementary Materials file.

490   **References:**

AAQS. (2012). National standard of the People's Republic of China GB3095-2012.
        https://www.mee.gov.cn/ywgz/fgbz/bz/bzwb/dqhjbh/dqhjzlbz/201203/W0201204103302323
        98521.pdf. Accessed 11 January, 2023.

Ainur, D., Chen, Q., Sha, T., Zarak, M., Dong, Z., Guo, W., Zhang, Z., Dina, K., An, T. (2023).
495   Outdoor Health Risk of Atmospheric Particulate Matter at Night in Xi'an, Northwestern
        China. *Environ Sci Technol*, 57, 9252-9265. https://doi.org/10.1021/acs.est.3c02670.

Alexandratos, N., Bruinsma, J., 2012. World agriculture towards 2030/2050, the 2012 revision
        (No. No. 12-03), ESA Working Paper. World Food and Agricultural Organization, Rome,
        Italy.

500   Brandt, J., Silver, J.D., Christensen, J.H., Andersen, M.S., B O Nl O Kke, J.H., Sigsgaard, T.,
        Geels, C., Gross, A., Hansen, A.B., Hansen, K.M., Hedegaard, G.B., Kaas, E., Frohn, L.M.
        (2013a). Contribution from the ten major emission sectors in Europe and Denmark to the
        health-cost externalities of air pollution using the EVA model system – an integrated
        modelling approach. *Atmos Chem Phys*, 13, 7725-7746. https://doi.org/10.5194/acp-13-7725-
505   2013.

Brandt, J., Silver, J.D., Christensen, J.H., Andersen, M.S., B O Nl O Kke, J.H., Sigsgaard, T.,
        Geels, C., Gross, A., Hansen, A.B., Hansen, K.M., Hedegaard, G.B., Kaas, E., Frohn, L.M.
        (2013b). Assessment of past, present and future health-cost externalities of air pollution in
        Europe and the contribution from international ship traffic using the EVA model system.
510   *Atmos Chem Phys*, 13, 7747-7764. https://doi.org/10.5194/acp-13-7747-2013.

Brandt, J., Silver, J.D., Frohn, L.M., Geels, C., Gross, A., Hansen, A.B., Hansen, K.M.,
        Hedegaard, G.B., Skjøth, C.A., Villadsen, H., Zare, A., Christensen, J.H. (2012). An
        integrated model study for Europe and North America using the Danish Eulerian Hemispheric
        Model with focus on intercontinental transport of air pollution. *Atmos Environ*, 53, 156-176.
515   https://doi.org/10.1016/j.atmosenv.2012.01.011.

Campbell, S.J., Wolfer, K., Utinger, B., Westwood, J., Zhang, Z.H., Bukowiecki, N., Steimer,
        S.S., Vu, T.V., Xu, J.S., Straw, N., Thomson, S., Elzein, A., Sun, Y.L., Liu, D., Li, L.J., Fu,
        P.Q., Lewis, A.C., Harrison, R.M., Bloss, W.J., Loh, M., Miller, M.R., Shi, Z.B., Kalberer,
        M. (2021). Atmospheric conditions and composition that influence PM2.5 oxidative potential
520   in Beijing, China. *Atmos Chem Phys*, 21, 5549-5573. https://doi.org/10.5194/acp-21-5549-
        2021.

CESM. (2023). Community Earth System Model. https://www.cesm.ucar.edu/. Accessed 7 May,
        2023.

Chen, L., Gao, Y., Ma, M., Wang, L., Wang, Q., Guan, S., Yao, X., Gao, H. (2023). Striking
525   impacts of biomass burning on PM2.5 concentrations in Northeast China through the
        emission inventory improvement. *Environ Pollut*, 318, 120835.
        https://doi.org/10.1016/j.envpol.2022.120835.

Chen, L., Wang, T., Bo, X., Zhuang, Z., Qu, J., Xue, X., Tian, J., Huang, M., Wang, P., Sang, M.
        (2022). Thermal Power Industry Emissions and Their Contribution to Air Quality on the Fen-
530   Wei Plain. *Atmosphere-Basel*, 13. https://doi.org/10.3390/atmos13050652.

Chen, P., Wang, T., Kasoar, M., Xie, M., Li, S., Zhuang, B., Li, M. (2018). Source Apportionment
        of PM2.5 during Haze and Non-Haze Episodes in Wuxi, China. *Atmosphere-Basel*, 9, 267.

https://doi.org/10.3390/atmos9070267.

Chen, T., Cao, S. (2021). Numerical study on the integrated effects of supplied air velocity and exhaust velocity on particles removal for industrial buildings. *Energy and Built Environment*, 2, 380-391. https://doi.org/10.1016/j.enbenv.2020.09.006.

Chen, T., Cao, S., Wang, J., Nizamani, A.G., Feng, Z., Kumar, P. (2021). Influences of the optimized air curtain at subway entrance to reduce the ingress of outdoor airborne particles. *Energ Buildings*, 244, 111028. https://doi.org/10.1016/j.enbuild.2021.111028.

Chen, Z.Y., Chen, D.L., Kwan, M.P., Chen, B., Gao, B.B., Zhuang, Y., Li, R.Y., Xu, B. (2019). The control of anthropogenic emissions contributed to 80% of the decrease in PM2.5 concentrations in Beijing from 2013 to 2017. *Atmos Chem Phys*, 19, 13519-13533. https://doi.org/10.5194/acp-19-13519-2019.

Christensen, J.H. (1997). The Danish eulerian hemispheric model — a three-dimensional air pollution model used for the arctic. *Atmos Environ*, 31, 4169-4191. https://doi.org/10.1016/S1352-2310(97)00264-1.

Cramer, J., Jorgensen, J.T., Hoffmann, B., Loft, S., Brauner, E.V., Prescott, E., Ketzel, M., Hertel, O., Brandt, J., Jensen, S.S., Backalarz, C., Simonsen, M.K., Andersen, Z.J. (2020). Long-Term Exposure to Air Pollution and Incidence of Myocardial Infarction: A Danish Nurse Cohort Study. *Environ Health Persp*, 128. https://doi.org/10.1289/EHP5818.

Crippa, M., Guizzardi, D., Butler, T., Keating, T., Wu, R., Kaminski, J., Kuenen, J., Kurokawa, J., Chatani, S., Morikawa, T., Pouliot, G., Racine, J., Moran, M.D., Klimont, Z., Manseau, P.M., Mashayekhi, R., Henderson, B.H., Smith, S.J., Suchyta, H., Muntean, M., Solazzo, E., Banja, M., Schaaf, E., Pagani, F., Woo, J.H., Kim, J., Monforti-Ferrario, F., Pisoni, E., Zhang, J., Niemi, D., Sassi, M., Ansari, T., Foley, K. (2023). The HTAP_v3 emission mosaic: merging regional and global monthly emissions (2000--2018) to support air quality modelling and policies. *Earth Syst Sci Data*, 15, 2667-2694. https://doi.org/10.5194/essd-15-2667-2023.

Danabasoglu, G., Lamarque, J.F., Bacmeister, J., Bailey, D.A., DuVivier, A.K., Edwards, J., Emmons, L.K., Fasullo, J., Garcia, R., Gettelman, A., Hannay, C., Holland, M.M., Large, W.G., Lauritzen, P.H., Lawrence, D.M., Lenaerts, J.T.M., Lindsay, K., Lipscomb, W.H., Mills, M.J., Neale, R., Oleson, K.W., Otto-Bliesner, B., Phillips, A.S., Sacks, W., Tilmes, S., van Kampenhout, L., Vertenstein, M., Bertini, A., Dennis, J., Deser, C., Fischer, C., Fox-Kemper, B., Kay, J.E., Kinnison, D., Kushner, P.J., Larson, V.E., Long, M.C., Mickelson, S., Moore, J.K., Nienhouse, E., Polvani, L., Rasch, P.J., Strand, W.G. (2020). The Community Earth System Model Version 2 (CESM2). *J Adv Model Earth Sy*, 12, e1916M-e2019M. https://doi.org/10.1029/2019MS001916.

de Melo, J.E., Pellicane, P.J., de Souza, M.R. (2000). Goodness-of-fit analysis on wood properties data from six Brazilian tropical hardwoods. *Wood Sci Technol*, 34, 83-97. https://doi.org/10.1007/s002260000033.

Eclipse. (2020). Global emission fields of air pollutants and GHGs. https://iiasa.ac.at/models-tools-data/global-emission-fields-of-air-pollutants-and-ghgs. Accessed 7 May, 2023.

Emery, C., Liu, Z., Russell, A.G., Odman, M.T., Yarwood, G., Kumar, N. (2017). Recommendations on statistics and benchmarks to assess photochemical model performance. *J Air Waste Manage*, 67, 582-598. https://doi-org.ez.statsbiblioteket.dk/10.1080/10962247.2016.1265027.

ERA. (2023). ECMWF Reanalysis v5. https://www.ecmwf.int/en/forecasts/dataset/ecmwf-

reanalysis-v5. Accessed 22 May, 2023.

Fang, T., Guo, H., Zeng, L., Verma, V., Nenes, A., Weber, R.J. (2017). Highly Acidic Ambient
Particles, Soluble Metals, and Oxidative Potential: A Link between Sulfate and Aerosol
580   Toxicity. *Environ Sci Technol*, 51, 2611-2620. https://doi.org/10.1021/acs.est.6b06151.

Gao, D., Pollitt, K., Mulholland, J.A., Russell, A.G., Weber, R.J. (2020). Characterization and
comparison of PM2.5 oxidative potential assessed by two acellular assays. *Atmos Chem Phys*,
20, 5197-5210. https://doi.org/10.5194/acp-20-5197-2020.

Geels, C., Andersson, C., Hänninen, O., Lansø, A.S., Schwarze, P.E., Skjøth, C.A., Brandt, J.
585   (2015). Future Premature Mortality Due to O3, Secondary Inorganic Aerosols and Primary
PM in Europe — Sensitivity to Changes in Climate, Anthropogenic Emissions, Population
and Building Stock. *Int J Env Res Pub He*, 12, 2837-2869.
https://doi.org/10.3390/ijerph120302837.

Geels, C., Winther, M., Andersson, C., Jalkanen, J.P., Brandt, J., Frohn, L.M., Im, U., Leung, W.,
590   Christensen, J.H. (2021). Projections of shipping emissions and the related impact on air
pollution and human health in the Nordic region. *Atmos Chem Phys*, 21, 12495-12519.
https://doi.org/10.5194/acp-21-12495-2021.

Gong, S., Zhang, L., Liu, C., Lu, S., Pan, W., Zhang, Y. (2022). Multi-scale analysis of the
impacts of meteorology and emissions on PM2.5 and O3 trends at various regions in China
595   from 2013 to 2020 2. Key weather elements and emissions. *Sci Total Environ*, 824, 153847.
https://doi.org/10.1016/j.scitotenv.2022.153847.

Hersbach, H., Bell, B., Berrisford, P., Hirahara, S., Horányi, A., Muñoz-Sabater, J., Nicolas, J.,
Peubey, C., Radu, R., Schepers, D., Simmons, A., Soci, C., Abdalla, S., Abellan, X.,
Balsamo, G., Bechtold, P., Biavati, G., Bidlot, J., Bonavita, M., De Chiara, G., Dahlgren, P.,
600   Dee, D., Diamantakis, M., Dragani, R., Flemming, J., Forbes, R., Fuentes, M., Geer, A.,
Haimberger, L., Healy, S., Hogan, R.J., Hólm, E., Janisková, M., Keeley, S., Laloyaux, P.,
Lopez, P., Lupu, C., Radnoti, G., de Rosnay, P., Rozum, I., Vamborg, F., Villaume, S.,
Thépaut, J. (2020). The ERA5 global reanalysis. *Q J Roy Meteor Soc*, 146, 1999-2049.
https://doi.org/10.1002/qj.3803.

605 Hodan, W.M., Barnard, W.R. (2004). Evaluating the contribution of PM2. 5 precursor gases and
re-entrained road emissions to mobile source PM2. 5 particulate matter emissions. *MACTEC
Federal Programs, Research Triangle Park, NC*.
https://www3.epa.gov/ttnchie1/conference/ei13/mobile/hodan.pdf.

IEA, 2011. World Energy Outlook 2011. International Energy Agency, Paris, France.

610 IEA, 2012. Energy Technology Perspectives. 2012 - Pathways to a Clean Energy System.
OECD/IEA, International Energy Agency, Paris.

Im, U., Bauer, S.E., Frohn, L.M., Geels, C., Tsigaridis, K., Brandt, J. (2023). Present-day and
future PM2.5 and O3-related global and regional premature mortality in the EVAv6.0 health
impact assessment model. *Environ Res*, 216, 114702.
615   https://doi.org/10.1016/j.envres.2022.114702.

Im, U., Brandt, J., Geels, C., Hansen, K.M., Christensen, J.H., Andersen, M.S., Solazzo, E.,
Kioutsioukis, I., Alyuz, U., Balzarini, A., Baro, R., Bellasio, R., Bianconi, R., Bieser, J.,
Colette, A., Curci, G., Farrow, A., Flemming, J., Fraser, A., Jimenez-Guerrero, P., Kitwiroon,
N., Liang, C.K., Nopmongcol, U., Pirovano, G., Pozzoli, L., Prank, M., Rose, R., Sokhi, R.,
620   Tuccella, P., Unal, A., Vivanco, M.G., West, J., Yarwood, G., Hogrefe, C., Galmarini, S.

(2018). Assessment and economic valuation of air pollution impacts on human health over Europe and the United States as calculated by a multi-model ensemble in the framework of AQMEII3. *Atmos Chem Phys*, 18, 5967-5989. https://doi.org/10.5194/acp-18-5967-2018.

625   Im, U., Christensen, J.H., Nielsen, O.K., Sand, M., Makkonen, R., Geels, C., Anderson, C., Kukkonen, J., Lopez-Aparicio, S., Brandt, J. (2019). Contributions of Nordic anthropogenic emissions on air pollution and premature mortality over the Nordic region and the Arctic. *Atmos Chem Phys*, 19, 12975-12992. https://doi.org/10.5194/acp-19-12975-2019.

Joint, R.C., Institute, F.E.A.S., Orlandini, L., Kurokawa, J., Monni, S., Akimoto, H., Grano, D., Battye, B., Zuber, A., Pagliari, V., Janssens-Maenhout, G., Van Aardenne, J., Dentener, F.,
630   Keating, T., Klimont, Z., Wankmüller, R., Ohara, T., 2011. EDGAR-HTAP – A harmonized gridded air pollution emission dataset based on national inventories. Publications Office.

Kumar, A., Patil, R.S., Dikshit, A.K., Kumar, R., Brandt, J., Hertel, O. (2016). Assessment of impact of unaccounted emission on ambient concentration using DEHM and AERMOD in combination with WRF. *Atmos Environ*, 142, 406-413.
635   https://doi.org/10.1016/j.atmosenv.2016.08.024.

Lehtomäki, H., Geels, C., Brandt, J., Rao, S., Yaramenka, K., Åström, S., Andersen, M.S., Frohn, L.M., Im, U., Hänninen, O. (2020). Deaths Attributable to Air Pollution in Nordic Countries: Disparities in the Estimates. *Atmosphere-Basel*, 11. https://doi.org/10.3390/atmos11050467.

Lin, S., Tian, H., Hao, Y., Wu, B., Liu, S., Luo, L., Bai, X., Liu, W., Zhao, S., Hao, J., Guo, Z.,
640   Lv, Y. (2021). Atmospheric emission inventory of hazardous air pollutants from biomass direct-fired power plants in China: Historical trends, spatial variation characteristics, and future perspectives. *Sci Total Environ*, 767, 144636. https://doi.org/10.1016/j.scitotenv.2020.144636.

Liu, J., Gao, X., Ruan, Z., Yuan, Y., Dong, S. (2022). Analysis of spatial and temporal distribution
645   and influencing factors of fine particles in Heilongjiang Province. *Urban Climate*, 41, 101070. https://doi.org/10.1016/j.uclim.2021.101070.

Liu, J., Ruan, Z., Gao, X., Yuan, Y., Dong, S. (2022). Quantifying contribution of weather patterns to PM2.5 concentrations based on spatial effects and health risk assessment. *Sustain Cities Soc*, 83, 103980. https://doi.org/10.1016/j.scs.2022.103980.

650   Liu, J., Ruan, Z., Gao, X., Yuan, Y., Dong, S., Li, X., Liu, X. (2023). Investigating the cumulative lag effects of environmental exposure under urban differences on COVID-19. *J Infect Public Heal*. https://doi.org/10.1016/j.jiph.2023.06.002.

Liu, M., Saari, R.K., Zhou, G., Li, J., Han, L., Liu, X. (2021). Recent trends in premature mortality and health disparities attributable to ambient PM2.5 exposure in China: 2005–
655   2017. *Environ Pollut*, 279, 116882. https://doi.org/10.1016/j.envpol.2021.116882.

Liu, Q., Lu, Z., Xiong, Y., Huang, F., Zhou, J., Schauer, J.J. (2020). Oxidative potential of ambient PM2.5 in Wuhan and its comparisons with eight areas of China. *Sci Total Environ*, 701, 134844. https://doi.org/10.1016/j.scitotenv.2019.134844.

Liu, S., Lim, Y., Pedersen, M., Jørgensen, J.T., Amini, H., Cole-Hunter, T., Mehta, A.J., So, R.,
660   Mortensen, L.H., Westendorp, R.G.J., Loft, S., Bräuner, E.V., Ketzel, M., Hertel, O., Brandt, J., Jensen, S.S., Christensen, J.H., Sigsgaard, T., Geels, C., Frohn, L.M., Brborić, M., Radonić, J., Sekulic, M.T., Bønnelykke, K., Backalarz, C., Simonsen, M.K., Andersen, Z.J. (2021). Long-term exposure to ambient air pollution and road traffic noise and asthma incidence in adults: The Danish Nurse cohort. *Environ Int*, 152, 106464.

665   https://doi.org/10.1016/j.envint.2021.106464.

Liu, W., Xu, Y., Liu, W., Liu, Q., Yu, S., Liu, Y., Wang, X., Tao, S. (2018). Oxidative potential of ambient PM2.5 in the coastal cities of the Bohai Sea, northern China: Seasonal variation and source apportionment. *Environ Pollut*, 236, 514-528. https://doi.org/10.1016/j.envpol.2018.01.116.

670   MEE. (2014). Ministry of Ecology and Environment. https://www.mee.gov.cn/. Accessed 11 January, 2023.

MEE. (2015). China Vehicle Emission Control Annual Report. https://www.mee.gov.cn/hjzl/sthjzk/ydyhjgl/201605/P020160513584304398771.pdf. Accessed 11 January, 2023.

675   MEE. (2020). Bulletin of the second National Survey of pollution sources. http://www.gov.cn/xinwen/2020-06/10/content_5518391.htm. Accessed 11 January, 2023.

Molina, C., Manzano, C.A., Toro A., R., Leiva G., M.A. (2023). The oxidative potential of airborne particulate matter in two urban areas of Chile: More than meets the eye. *Environ Int*, 173, 107866. https://doi.org/10.1016/j.envint.2023.107866.

680   Pui, D.Y.H., Chen, S., Zuo, Z. (2014). PM2.5 in China: Measurements, sources, visibility and health effects, and mitigation. *Particuology*, 13, 1-26. https://doi.org/10.1016/j.partic.2013.11.001.

Shahpoury, P., Lelieveld, S., Johannessen, C., Berkemeier, T., Celo, V., Dabek-Zlotorzynska, E., Harner, T., Lammel, G., Nenes, A. (2024). Influence of aerosol acidity and organic ligands on
685   transition metal solubility and oxidative potential of fine particulate matter in urban environments. *Sci Total Environ*, 906, 167405. https://doi.org/10.1016/j.scitotenv.2023.167405.

Skamarock, W.C., Klemp, J.B., Dudhia, J., Gill, D.O., Barker, D.M., Duda, M.G., Huang, X., Wang, W., Powers, J.G. (2008). A description of the advanced research WRF version 3.
690   *NCAR technical note*, 475, 113. http://dx.doi.org/10.5065/D68S4MVH.

Tang, L., Xue, X., Qu, J., Mi, Z., Bo, X., Chang, X., Wang, S., Li, S., Cui, W., Dong, G. (2020). Air pollution emissions from Chinese power plants based on the continuous emission monitoring systems network. *Sci Data*, 7, 325. https://doi.org/10.1038/s41597-020-00665-1.

Thomas, D.C., Christensen, J.H., Massling, A., Pernov, J.B., Skov, H. (2022). The effect of the
695   2020 COVID-19 lockdown on atmospheric black carbon levels in northeastern Greenland. *Atmos Environ*, 269, 118853. https://doi.org/10.1016/j.atmosenv.2021.118853.

Tong, D., Zhang, Q., Liu, F., Geng, G., Zheng, Y., Xue, T., Hong, C., Wu, R., Qin, Y., Zhao, H., Yan, L., He, K. (2018). Current Emissions and Future Mitigation Pathways of Coal-Fired Power Plants in China from 2010 to 2030. *Environ Sci Technol*, 52, 12905-12914.
700   https://doi.org/10.1021/acs.est.8b02919.

Upadhyay, A., Dey, S., Goyal, P. (2020). A comparative assessment of regional representativeness of EDGAR and ECLIPSE emission inventories for air quality studies in India. *Atmos Environ*, 223, 117182. https://doi.org/10.1016/j.atmosenv.2019.117182.

van Donkelaar, A., Hammer, M.S., Bindle, L., Brauer, M., Brook, J.R., Garay, M.J., Hsu, N.C.,
705   Kalashnikova, O.V., Kahn, R.A., Lee, C., Levy, R.C., Lyapustin, A., Sayer, A.M., Martin, R.V. (2021). Monthly Global Estimates of Fine Particulate Matter and Their Uncertainty. *Environ Sci Technol*, 55, 15287-15300. https://doi.org/10.1021/acs.est.1c05309.

Wang, G., Deng, J., Zhang, Y., Zhang, Q., Duan, L., Hao, J., Jiang, J. (2020). Air pollutant

emissions from coal-fired power plants in China over the past two decades. *Sci Total Environ*,
741, 140326. https://doi.org/10.1016/j.scitotenv.2020.140326.

Wang, J., Lin, X., Lu, L., Wu, Y., Zhang, H., Lv, Q., Liu, W., Zhang, Y., Zhuang, S. (2019).
Temporal variation of oxidative potential of water soluble components of ambient PM2.5
measured by dithiothreitol (DTT) assay. *Sci Total Environ*, 649, 969-978.
https://doi.org/10.1016/j.scitotenv.2018.08.375.

Xing, C., Wang, Y., Yang, X., Zeng, Y., Zhai, J., Cai, B., Zhang, A., Fu, T., Zhu, L., Li, Y.,
Wang, X., Zhang, Y. (2023). Seasonal variation of driving factors of ambient PM2.5
oxidative potential in Shenzhen, China. *Sci Total Environ*, 862, 160771.
https://doi.org/10.1016/j.scitotenv.2022.160771.

Yu, S., Liu, W., Xu, Y., Yi, K., Zhou, M., Tao, S., Liu, W. (2019). Characteristics and oxidative
potential of atmospheric PM2.5 in Beijing: Source apportionment and seasonal variation. *Sci
Total Environ*, 650, 277-287. https://doi.org/10.1016/j.scitotenv.2018.09.021.

Yun, X., Shen, G.F., Shen, H.Z., Meng, W.J., Chen, Y.L., Xu, H.R., Ren, Y., Zhong, Q.R., Du,
W., Ma, J.M., Cheng, H.F., Wang, X.L., Liu, J.F., Wang, X.J., Li, B.G., Hu, J.Y., Wan, Y.,
Tao, S. (2020). Residential solid fuel emissions contribute significantly to air pollution and
associated health impacts in China. *Sci Adv*, 6. https://www-science-
org.ez.statsbiblioteket.dk/doi/10.1126/sciadv.aba7621.

Zare, A., Christensen, J.H., Gross, A., Irannejad, P., Glasius, M., Brandt, J. (2014). Quantifying
the contributions of natural emissions to ozone and total fine PM concentrations in the
Northern Hemisphere. *Atmos Chem Phys*, 14, 2735-2756. https://doi.org/10.5194/acp-14-
2735-2014.

Zeng, Z., Gui, K., Wang, Z., Luo, M., Geng, H., Ge, E., An, J., Song, X., Ning, G., Zhai, S., Liu,
H. (2021). Estimating hourly surface PM2.5 concentrations across China from high-density
meteorological observations by machine learning. *Atmos Res*, 254, 105516.
https://doi.org/10.1016/j.atmosres.2021.105516.

Zhang, H., Li, N., Tang, K., Liao, H., Shi, C., Huang, C., Wang, H., Guo, S., Hu, M., Ge, X.
(2022). Estimation of secondary PM 2.5 in China and the United States using a multi-tracer
approach. *Atmos Chem Phys*, 22, 5495-5514. https://doi.org/10.5194/acp-2021-683.

Zhang, L., Hu, X., Chen, S., Chen, Y., Lian, H. (2023). Characterization and source apportionment
of oxidative potential of ambient PM2.5 in Nanjing, a megacity of Eastern China.
Environmental Pollutants and Bioavailability, 35, 2175728.
https://doi.org/10.1080/26395940.2023.2175728.

Zhang, Z., Gao, J., Zhang, L., Wang, H., Tao, J., Qiu, X., Chai, F., Li, Y., Wang, S. (2017).
Observations of biomass burning tracers in PM2.5 at two megacities in North China during
2014 APEC summit. *Atmos Environ*, 169, 54-64.
https://doi.org/10.1016/j.atmosenv.2017.09.011.

Zheng, B., Tong, D., Li, M., Liu, F., Hong, C.P., Geng, G.N., Li, H.Y., Li, X., Peng, L.Q., Qi, J.,
Yan, L., Zhang, Y.X., Zhao, H.Y., Zheng, Y.X., He, K.B., Zhang, Q. (2018). Trends in
China's anthropogenic emissions since 2010 as the consequence of clean air actions. *Atmos
Chem Phys*, 18, 14095-14111. https://doi.org/10.5194/acp-18-14095-2018.

Zhu, Y., Huang, L., Li, J., Ying, Q., Zhang, H., Liu, X., Liao, H., Li, N., Liu, Z., Mao, Y., Fang,
H., Hu, J. (2018). Sources of particulate matter in China: Insights from source apportionment
studies published in 1987 – 2017. *Environ Int*, 115, 343-357.

https://doi.org/10.1016/j.envint.2018.03.037.